Basal CHK1 activity safeguards its stability to maintain intrinsic S-phase checkpoint functions

Jone Michelena[1], Marco Gatti[1], Federico Teloni[1,2], Ralph Imhof[1], and Matthias Altmeyer[1]

The DNA replication machinery frequently encounters impediments that slow replication fork progression and threaten timely and error-free replication. The CHK1 protein kinase is essential to deal with replication stress (RS) and ensure genome integrity and cell survival, yet how basal levels and activity of CHK1 are maintained under physiological, unstressed conditions is not well understood. Here, we reveal that CHK1 stability is controlled by its steady-state activity during unchallenged cell proliferation. This autoactivatory mechanism, which depends on ATR and its coactivator ETAA1 and is tightly associated with CHK1 autophosphorylation at S296, counters CHK1 ubiquitylation and proteasomal degradation, thereby preventing attenuation of S-phase checkpoint functions and a compromised capacity to respond to RS. Based on these findings, we propose that steady-state CHK1 activity safeguards its stability to maintain intrinsic checkpoint functions and ensure genome integrity and cell survival.

Introduction

The genome is constantly exposed to different sources of harmful agents, both endogenous and exogenous, which can interfere with the DNA replication machinery, leading to replication stress (RS) and DNA damage (Zeman and Cimprich, 2014; Saldivar et al., 2017; Técher et al., 2017). Mild forms of RS occur during physiological cell cycle progression, and pathological events such as oncogene activation further elevate RS, promoting genome instability and cancer development (Gaillard et al., 2015). Markers of persistent RS can be observed in most cancers and, therefore, defining how mammalian cells deal with RS and understanding how the RS response is deregulated in cancer may reveal cancer-specific vulnerabilities that can be exploited for cancer therapy (Dobbelstein and Sørensen, 2015; Jackson and Helleday, 2016).

Ataxia telangiectasia and Rad3-related (ATR) is the apical kinase that responds to RS, and its activity is required to suppress RS-associated DNA damage (Yazinski and Zou, 2016; Blackford and Jackson, 2017). ATR functions are essential even during normal, unperturbed cell proliferation, and were recently shown to enforce a minimum threshold of replication before allowing the onset of mitosis (Sørensen and Syljuåsen, 2012; Eykelenboom et al., 2013; Saldivar et al., 2018). Upon induced RS, ATR is recruited and activated by replication protein A (RPA) bound to single-stranded DNA (ssDNA). Full kinase activation depends on activator proteins, and in vertebrates two ATR activators have been identified, topoisomerase II binding protein 1 (TOPBP1) and Ewing tumor–associated antigen 1 (ETAA1), which are both recruited to stalled replication forks through direct interactions with RPA (Bass et al., 2016; Haahr et al., 2016; Lee et al., 2016). Depletion of TOPBP1 and ETAA1 was shown to be synthetic lethal, suggesting that these two ATR activating proteins act in parallel and distinct pathways of ATR activation (Bass et al., 2016; Haahr et al., 2016). Whether these parallel pathways resemble distinct RS inputs is currently not known.

Instrumental to the ATR-mediated response to RS is the downstream effector kinase CHK1, which, by controlling replication origin firing, delaying cell cycle progression, and stabilizing stalled replication forks, creates a time window to resolve DNA lesions, and ensures that cells do not enter mitosis when replication is incomplete (Schmitt et al., 2006; Maya-Mendoza et al., 2007; Ge and Blow, 2010; González Besteiro and Gottifredi, 2015; Smits and Gillespie, 2015; Toledo et al., 2017). CHK1 loss or inactivation causes lethality (Liu et al., 2000; Takai et al., 2000), suggesting that CHK1, similar to ATR, is active during normal cell cycle progression even in the absence of exogenous RS. CHK1 activity and stability have been mainly studied upon excessive RS and in the context of checkpoint adaptation (den Elzen and O'Connell, 2004; Zhang et al., 2005, 2009; Mailand et al., 2006; Mamely et al., 2006; Peschiaroli et al., 2006; Collis

....

[1]Department of Molecular Mechanisms of Disease, University of Zurich, Zurich, Switzerland; [2]Molecular Life Sciences Program, Life Science Zurich Graduate School, Zurich, Switzerland.

Correspondence to Matthias Altmeyer: matthias.altmeyer@uzh.ch.

et al., 2007; Leung-Pineda et al., 2009; Huh and Piwnica-Worms, 2013; Alonso-de Vega et al., 2014; Park et al., 2015; Liu et al., 2017; Tu et al., 2017; Cheng and Shieh, 2018; Ito et al., 2018; Deshar et al., 2019), and the cellular mechanisms that regulate steady-state CHK1 functions and how they impact replication dynamics have remained elusive.

Here, we report an autoactivatory loop through which basal CHK1 activity safeguards its stability in order to maintain intrinsic checkpoint functions. Failure to sustain CHK1 autophosphorylation results in its rapid proteasomal degradation, checkpoint malfunction, and impaired ability to respond to RS. We propose that this mechanism of intrinsic checkpoint abrogation can initiate a vicious cycle and may provide a means to eliminate checkpoint defective cells from the proliferative pool, thereby guarding against cellular transformation and cancer development.

Results and discussion

To evaluate the cellular mechanisms that ensure essential replication checkpoint functions under unchallenged conditions, we modulated CHK1 activity in U-2 OS cells by short-term exposure to the small molecule CHK1 inhibitors (CHK1i) UCN-01 and CHIR-124. We monitored basal CHK1 activity by assessing CHK1 phosphorylation at its residue S296 (pCHK1 S296), an autophosphorylation site tightly associated with CHK1 activation (Kasahara et al., 2010; Okita et al., 2012; González Besteiro and Gottifredi, 2015), in parallel to the DNA damage markers phospho-KAP1 (pKAP1 S824) and phospho-RPA (pRPA S4/8). In line with previous reports (Syljuåsen et al., 2005; Shen et al., 2015), treating cells with typically used concentrations of UCN-01(300 nM) and CHIR-124 (50 nM) led to a strong induction of DNA damage (Fig. 1, A and B). Similar results were obtained when we transiently depleted CHK1 by siRNA (Fig. S1 A). To experimentally uncouple interrogations of checkpoint functions by this essential kinase from the DNA damage caused by complete loss of its activity, we titrated CHK1i and monitored basal CHK1 activity and markers of DNA damage under these conditions. 10-fold lower concentrations of CHK1i indeed led to reduced CHK1 autophosphorylation at S296 without any signs of DNA damage (Fig. 1, A and B; and see below). Such conditions therefore provide an opportunity to assess intrinsic checkpoint functions and mechanisms of CHK1 regulation without interference from CHK1i-induced DNA damage. Unexpectedly, we found that under these conditions of CHK1 inhibition, protein levels of CHK1 were also markedly decreased (Fig. 1, A and B). This reduction in CHK1 protein levels following CHK1 inhibition occurred gradually over time and, upon extended treatment duration, eventually resulted in DNA damage, similar to CHK1 depletion (Fig. S1 B).

Next, to determine at the single cell level and in a quantitative manner how CHK1 activity impacts its protein levels in the absence of DNA damage, we established conditions to assess CHK1 steady-state activity and protein levels in conjunction with markers of RS and DNA damage signaling by quantitative image-based cytometry (QIBC; Altmeyer et al., 2013; Toledo et al., 2013). The observed signals for CHK1 and pCHK1 S296

were specific as revealed by transient CHK1 depletion experiments with and without hydroxyurea (HU)-induced CHK1 activation (Fig. S1, C–E). Based on this approach, cells treated with a low concentration (30 nM) of CHK1i showed a decrease in CHK1 activity as measured by pCHK1 S296 staining (Fig. 1 C), without DNA replication being compromised (Fig. 1 D) and without significant increase in γH2AX (Fig. 1 E), pRPA, and pKAP1 (Fig. S1, F and G). As expected, treatment with high concentrations of CHK1i resulted in catastrophic DNA damage in S-phase and decreased DNA replication capacity (Fig. 1, D and E; and Fig. S1, F and G). Moreover, we found that inhibition of CHK1 basal activity with low doses of CHK1i was coupled to a clear reduction in CHK1 protein levels (Fig. 1 F). This reduction was not restricted to S-phase cells but rather occurred throughout the cell cycle and was evident as early as 30 min after CHK1i (Fig. 1 G and Fig. S1, H–J). After such short-term CHK1i, we did not observe a measurable increase in entry into mitosis, while longer CHK1i (8 h) resulted in accelerated mitotic entry (Fig. 1 H). Addition of the CDK inhibitor roscovitine reverted the accelerated mitotic entry (Fig. 1 H), yet did not rescue CHK1 levels upon CHK1i (Fig. 1 I), suggesting that the observed CHK1 loss was unrelated to premature mitotic entry. Reduced CHK1 levels upon CHK1i were also obtained in a nontransformed cell line (Fig. S1, K–O). CHK1 mRNA levels, on the other hand, were unaffected by low-dose CHK1i (Fig. S1 P). Taken together, these results indicate that CHK1 steady-state activity in unstressed conditions controls CHK1 protein levels.

CHK1 activity is regulated by the upstream kinase ATR (Smits and Gillespie, 2015). ATR depletion by siRNA suppressed CHK1 activity and also decreased total CHK1 protein levels, measured by both QIBC and Western blot, without adverse effects on DNA replication (Fig. S2, A–D). To directly test whether steady-state CHK1 activity promotes its stability, we first measured the half-life of CHK1 in cells treated or not with CHK1i in the presence of cycloheximide, an inhibitor of protein synthesis commonly used for protein half-life measurements. These experiments revealed that CHK1 was indeed much less stable in CHK1i-treated cells (with a half-life of ~2 h) as compared with control cells (Fig. 2 A). Next, we treated cells with CHK1i together with the proteasome inhibitor MG132 to block protein degradation. Reassuringly, CHK1 protein levels in CHK1i-treated cells were rescued almost to control conditions when proteasomal degradation was suppressed (Fig. 2 B). Collectively, these data provide evidence that steady-state CHK1 activity influences its own stability by preventing its proteasomal degradation.

To further test this notion, we assessed whether CHK1i would affect CHK1 ubiquitylation. These experiments revealed that CHK1 ubiquitylation was indeed elevated in cells treated with low-dose CHK1i (Fig. 2 C). Previous studies demonstrated that upon prolonged genotoxic stress treatments, the CUL1- and CUL4A-containing E3 ubiquitin ligase complexes mediate CHK1 ubiquitylation and proteasomal degradation, and identified DDB1 as the adapter protein that targets the ubiquitin ligase complex to CHK1 (Zhang et al., 2005, 2009; Leung-Pineda et al., 2009; Ma et al., 2018). We therefore assessed whether DDB1 might also control CHK1 degradation upon impaired basal activity in the absence of exogenous RS. Indeed, depletion of DDB1
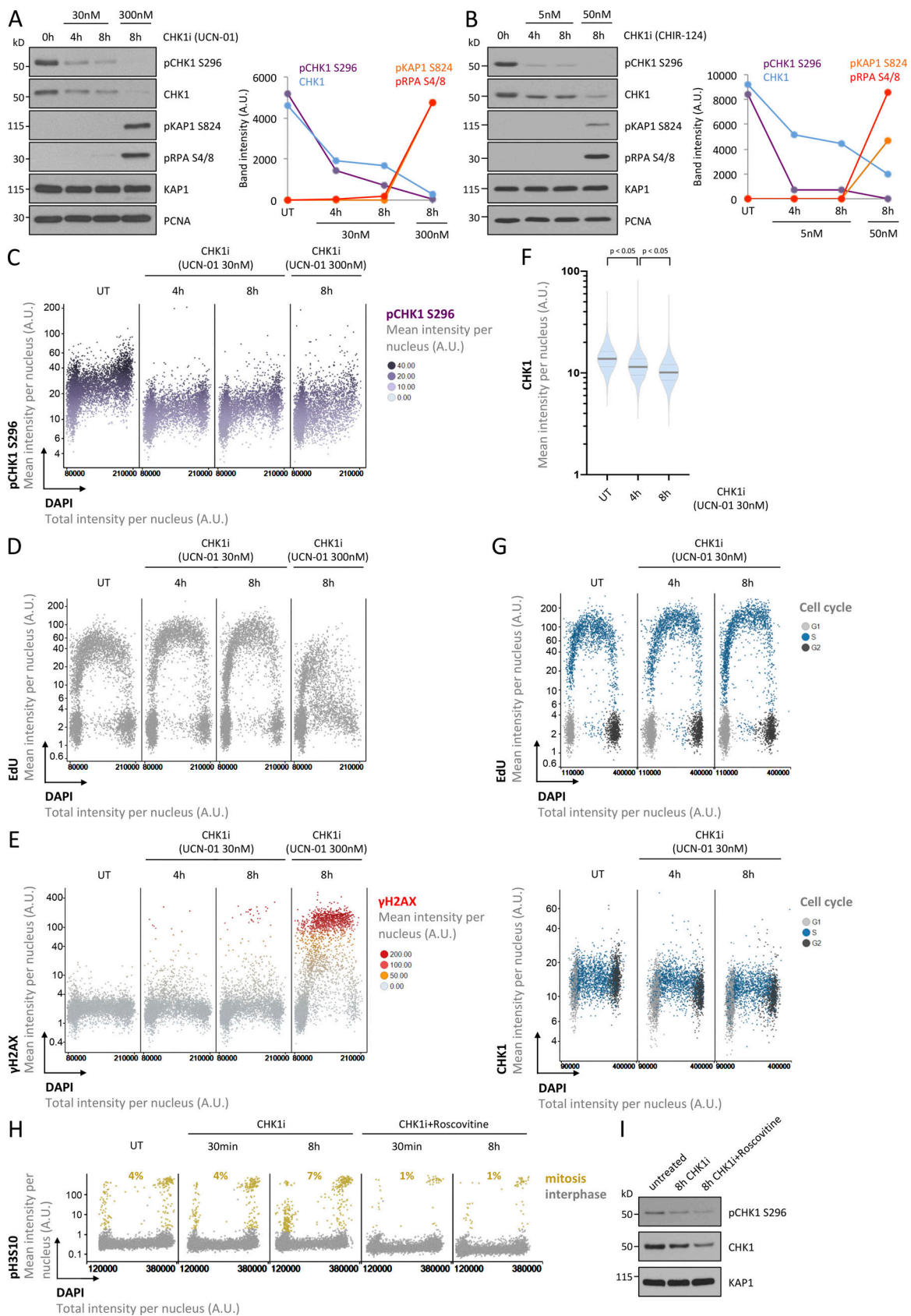
Michelena et al.
Basal CHK1 activity maintains its stability

Journal of Cell Biology 2866
https://doi.org/10.1083/jcb.201902085

Figure 1. **Steady-state CHK1 activity maintains CHK1 levels in unchallenged conditions. (A)** Western blot analysis of asynchronously growing populations of U-2 OS cells treated with a low (30 nM) or high (300 nM) concentration of CHK1i UCN-01 as indicated. The band intensities were quantified by ImageJ and are depicted to the right. **(B)** Western blot analysis of U-2 OS cells treated with a low (5 nM) or high (50 nM) concentration of CHK1i CHIR-124 as indicated. The

band intensities were quantified by ImageJ and are depicted to the right. **(C)** QICB analysis of U-2 OS cells treated with CHK1i as indicated and stained for pCHK1 S296, γH2AX, EdU, and DNA content (sample size: 5,092, 5,054, 4,992, and 5,276 cells). **(D)** Cell cycle–resolved EdU levels from cells in C. **(E)** γH2AX levels from the staining in C and D. **(F)** U-2 OS cells were treated with CHK1i as indicated and stained for CHK1, γH2AX, EdU, and DNA content. QIBC-derived analysis of CHK1 levels is depicted with median (solid line) and quartiles (dashed lines) indicated (sample size: 3,303, 3,507, and 3,985 cells). **(G)** Cell cycle–resolved EdU and CHK1 levels from cells in F. **(H)** U-2 OS cells were treated with CHK1i (30 nM UCN-01) with or without roscovitine (20 μM) for 30 min or 8 h as indicated, stained for the mitotic marker phospho-H3 S10 (pH3S10) and DNA content, and analyzed by QIBC with percentages of cells in mitosis indicated (sample size: 4,916, 5,040, 4,936, 5,152, and 5,025 cells). **(I)** Western blot analysis of cells treated with CHK1i and roscovitine as in H for 8 h. Mann–Whitney U test in F. A.U., arbitrary units.

stabilized CHK1 under basal conditions and also restored CHK1 levels from CHK1i-mediated degradation (Fig. 2 D), suggesting that DDB1 participates in CHK1 degradation upon loss of steady-state CHK1 activity.

Our findings so far suggest that steady-state activity of CHK1 prevents its ubiquitylation and proteasomal degradation to maintain physiological CHK1 levels and to ensure essential CHK1 functions. To directly test the requirement of CHK1 autophosphorylation
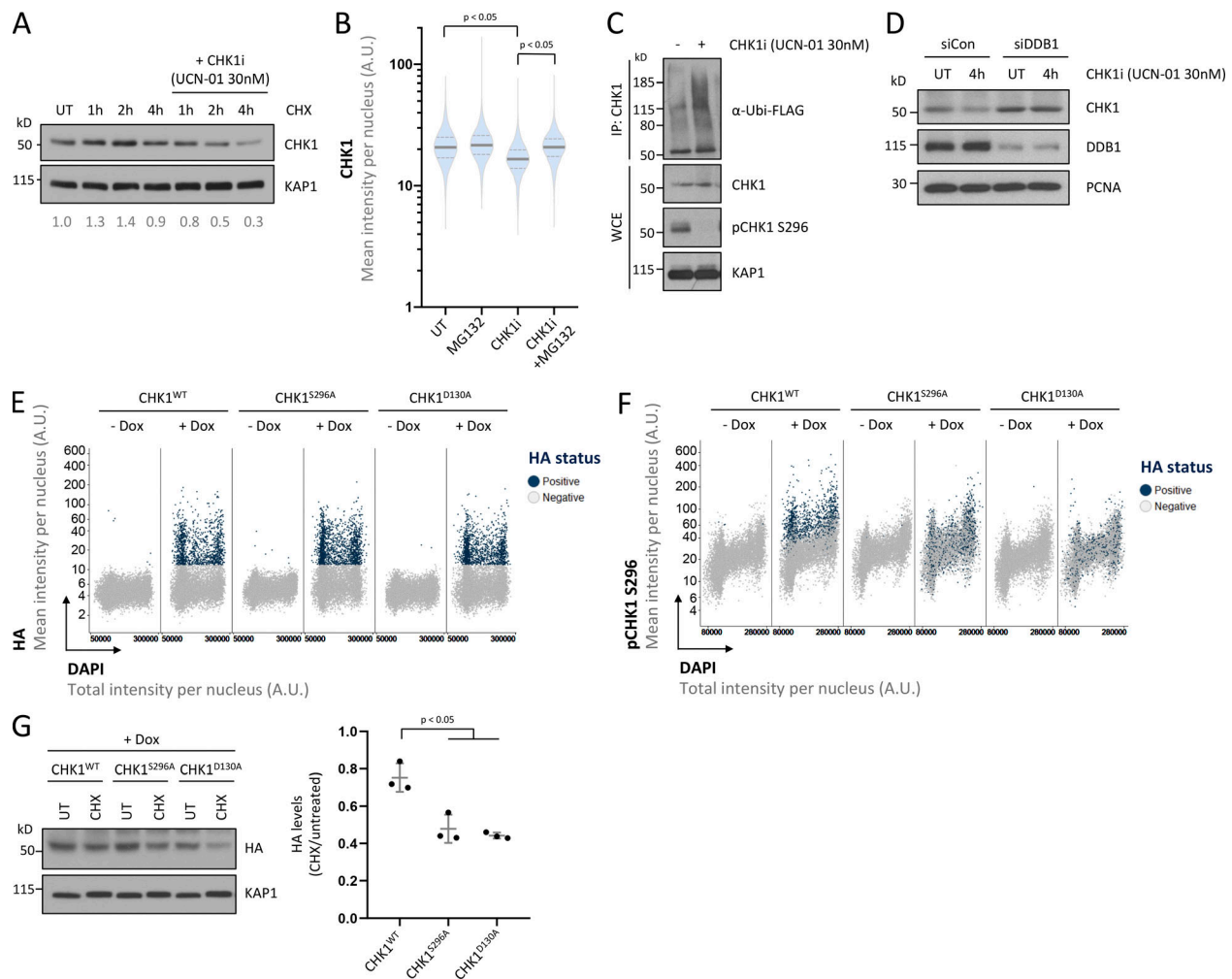

Figure 2. **CHK1 inhibition accelerates CHK1 proteasomal degradation. (A)** U-2 OS cells treated or not with low-dose CHK1i were exposed to cycloheximide (CHX), collected at indicated time points, and immunoblotted with CHK1- and KAP1-recognizing antibodies to assess CHK1 half-life with and without CHK1i. **(B)** U-2 OS cells were exposed to low-dose CHK1i and the proteasome inhibitor MG132 for 2 h as indicated and stained for CHK1. QIBC-derived levels of CHK1 are shown with median (solid line) and quartiles (dashed lines) indicated (sample size: 3,915, 3,938, 3,594, and 3,772 cells). **(C)** U-2 OS cells were transfected with a ubiquitin-FLAG (Ubi-FLAG) expressing plasmid, and treated with MG132 and low-dose CHK1i for 4 h as indicated, and endogenous CHK1 was immunoprecipitated with a CHK1-recognizing antibody. Immunoprecipitates were blotted with FLAG antibody to detect ubiquitylated CHK1. IP, immunoprecipitation; WCE, whole cell extract. **(D)** U-2 OS cells were transfected with negative control siRNA or siRNA against DDB1 for 48 h, treated with low-dose CHK1i and MG132 for 4 h, and blotted with CHK1, DDB1, and PCNA antibodies. **(E)** U-2 OS cells expressing either WT CHK1-HA, CHK1-HA S296A, or CHK1-HA D130A upon doxycycline (Dox) addition for 24 h were analyzed by QIBC for their HA-signal (sample size: 8,001, 8,118, 7,042, 7,718, 8,396, and 8,695 cells). **(F)** In the same cells from E, pCHK1 S296 was analyzed. **(G)** Western blot analysis of U-2 OS expressing WT CHK1-HA, CHK1-HA S296A, or CHK1-HA D130A treated with CHX for 1 h as indicated. A representative Western blot is shown together with quantifications of relative HA intensities from Western blots of three independent experiments with means ± SD indicated. Mann–Whitney U test in B, unpaired t test in G. A.U., arbitrary units.

Michelena et al.
Basal CHK1 activity maintains its stability

Journal of Cell Biology
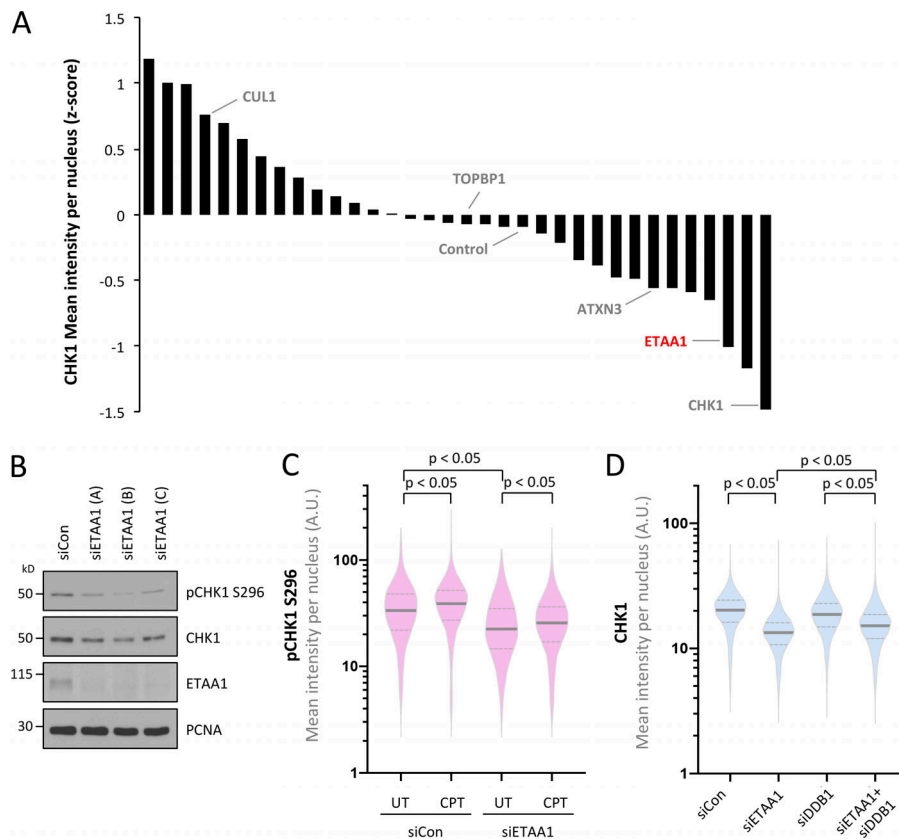https://doi.org/10.1083/jcb.201902085

2868

Figure 3. **A high-content microscopy-based screen identifies the ATR activator ETAA1 as a novel regulator of CHK1 stability. (A)** Targeted siRNA screen for modulators of CHK1 levels. Three independent siRNAs were used against each target gene for 48 h, the results were averaged, and z-scores according to CHK1 levels are shown. On average, 4,300 cells were analyzed by QIBC for each gene. **(B)** Western blot analysis of pCHK1 S296 and total CHK1 levels in U-2 OS cells transfected for 48 h with three independent siRNAs against ETAA1. **(C)** U-2 OS cells were transfected with siETAA1 (A) for 48 h, treated with CPT (1 µM) for 1 h, and stained for pCHK1 S296. QIBC-derived levels of pCHK1 S296 are shown with median (solid line) and quartiles (dashed lines) indicated (sample size: 2,599, 4,791, 3,210, and 5,009 cells). **(D)** U-2 OS cells were transfected with siETAA1 (A) and siDDB1 for 48 h as indicated and stained for CHK1. QIBC-derived levels of CHK1 are shown with median (solid line) and quartiles (dashed lines) indicated (sample size: 6,819, 6,592, 6,723, and 6,772 cells). Mann–Whitney U test in C and D. A.U., arbitrary units.

for its stability, we generated stable cell lines expressing in an inducible manner either WT CHK1, a CHK1 S296A mutant, or a catalytically inactive CHK1 D130A mutant (Chen et al., 2000). The three proteins, carrying an HA tag for detection, were expressed at comparable levels upon induction (Fig. 2 E). Reassuringly, only WT CHK1 expression resulted in an increase in pCHK1 S296, while both the S296A and the D130A mutants were defective in this modification (Fig. 2 F). Both mutants were consistently less stable than the WT counterpart, providing evidence that loss of catalytic activity and S296 autophosphorylation promote CHK1 turnover (Fig. 2 G). We therefore conclude that CHK1 autophosphorylation is needed to maintain its stability in unperturbed conditions.

Given the essential genome maintenance function of CHK1, we aimed to identify upstream factors, which would modulate CHK1 steady-state activity and stability in unchallenged conditions. To this end, we performed a high-content microscopy-based screen using a targeted, custom-designed siRNA library comprising genes with known roles in genome integrity maintenance and ATR/CHK1 regulation and assessed CHK1 levels and γH2AX. Among the factors whose depletion led to lower CHK1 levels, we identified Ataxin-3 (Fig. 3 A and Table S1), a deubiquitinase that was previously shown to suppress CHK1 ubiquitylation and proteasomal degradation (Tu et al., 2017). Interestingly, we also identified ETAA1 as a putative positive regulator of CHK1 levels (Fig. 3 A). ETAA1 is an ATR activator, which was recently shown to regulate the S/G2 transition in normally proliferating cells (Saldivar et al., 2018). We thus considered the possibility that ETAA1 might control CHK1 levels in unchallenged cells. We validated the screen results using

different siRNAs against ETAA1 and assessing CHK1 levels by Western blot (Fig. 3 B), and confirmed that CHK1 levels were reduced upon ETAA1 depletion in different transformed and nontransformed cell lines (Fig. S2, E and F). Importantly, the half-life of CHK1 was also reduced in multiple cell lines upon ETAA1 depletion, supporting a role of ETAA1 in maintaining CHK1 protein stability (Fig. S2, G–I). We next tested the possibility that ETAA1 might regulate CHK1 levels by promoting its basal activation state in unchallenged conditions. Indeed, steady-state pCHK1 S296 was reduced in ETAA1-depleted cells, while RS-induced CHK1 activation was only mildly impaired (Fig. 3 C and Fig. S2, J and K). In contrast, depletion of the second known ATR activator protein, TOPBP1, which did not score in our initial screen (Fig. 3 A), only mildly affected CHK1 levels, its half-life, and steady-state activity, despite the fact that it strongly reduced CHK1 activation after exogenous RS (Fig. S2, L–O). The reduced CHK1 protein levels upon ETAA1 depletion were partly restored by DDB1 codepletion (Fig. 3 D and Fig. S2 P), indicating that by ensuring CHK1 activity, ETAA1 abrogates DDB1-mediated CHK1 proteasomal degradation. Taken together, our results suggest that impaired basal CHK1 activity, either at the level of CHK1 activation itself or at the level of upstream signaling through ATR/ETAA1 (and, under unchallenged conditions, to a lesser extent through ATR/TOPBP1), leads to rapid proteasomal degradation of CHK1 and reduces CHK1 levels.

Finally, we asked what the cellular consequences are of impaired CHK1 autoactivation and destabilization. Loss of CHK1 resulted in increased levels of the RS sensor and negative cell cycle regulator p21 before DNA damage signaling (Fig. S3, A and B),
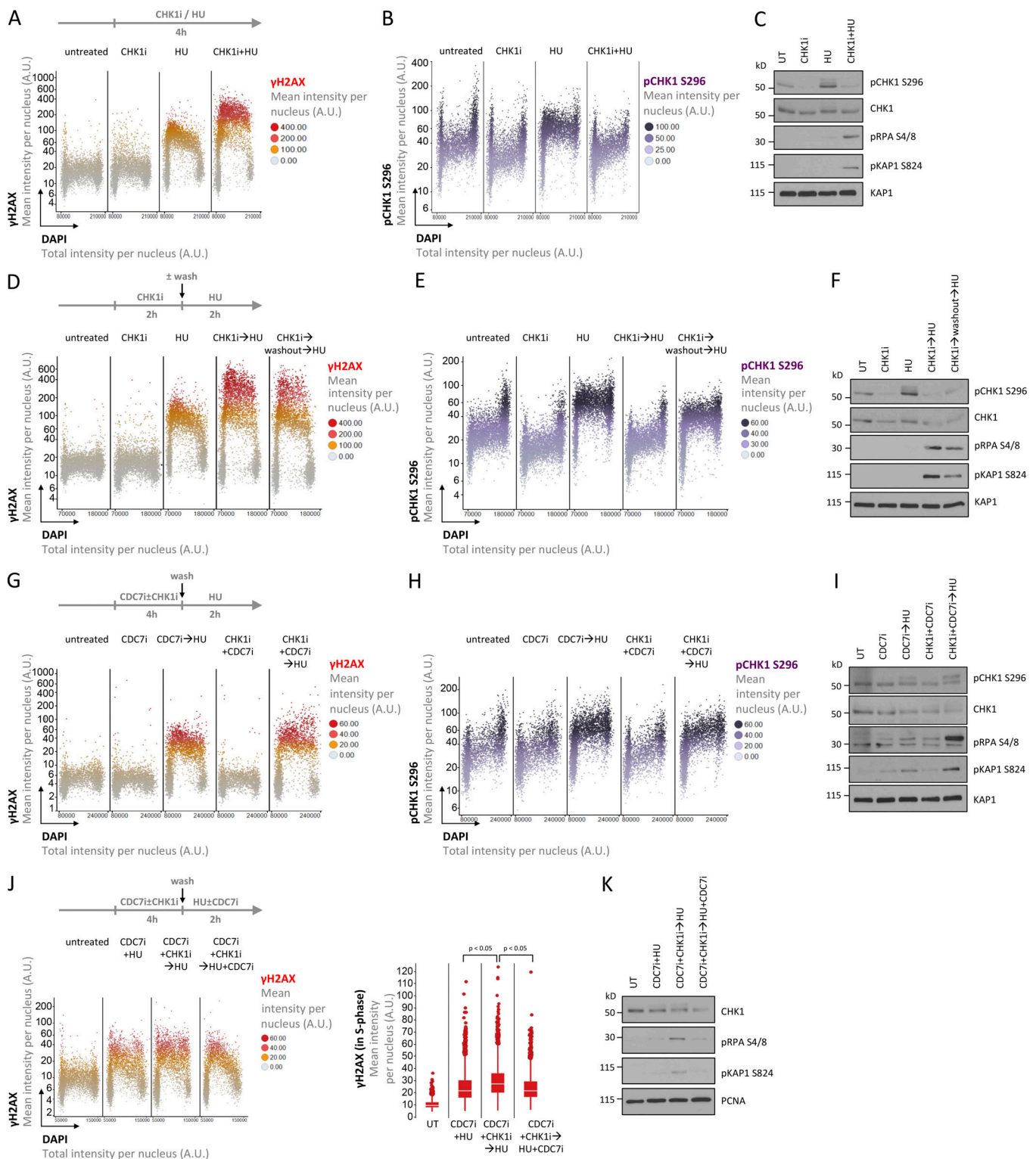
Figure 4. **CHK1 degradation upon impaired steady-state activity sensitizes to RS. (A)** U-2 OS cells were treated as indicated for 4 h with low-dose CHK1i, 2mM HU, or both, and stained for γH2AX, pCHK1 S296 and DNA content. QIBC-derived γH2AX profiles are shown (sample size: 4,896, 5,153, 5,005, and 5,187 cells). **(B)** pCHK1 S296 profiles from the staining in A are shown. **(C)** Western blot analysis of DNA damage markers in cells treated as indicated for 4 h with low-dose CHK1i, 2 mM HU, or both. **(D)** U-2 OS cells were treated with low-dose CHK1i for 2 h, the inhibitor was washed out, and the cells were then treated with 2 mM HU for an additional 2 h. Cells were stained for γH2AX, pCHK1 S296, and DNA content. QIBC-derived γH2AX profiles are shown (sample size: 5,388, 5,187, 4,190, 4,831, and 5,060 cells). **(E)** pCHK1 S296 profiles from the staining in D are shown. **(F)** Western blot analysis of DNA damage markers in cells treated as in D and E. **(G)** U-2 OS cells were treated with CDC7i to block origin firing in the presence or absence of low-dose CHK1i for 4 h, the drugs were removed, and cells were then exposed to 2 mM HU for 2 h. Cells were stained for γH2AX, pCHK1 S296, and DNA content. QIBC-derived γH2AX profiles are shown (sample size: 3,147, 3,177, 3,757, 2,656, and 3,524 cells). **(H)** pCHK1 S296 profiles from the staining in G are shown. **(I)** Western blot analysis of DNA

damage markers in cells treated as in G and H. **(J)** U-2 OS cells were treated with CDC7i in the presence or absence of low-dose CHK1i for 4 h, the drugs were removed, and cells were then exposed to 0.5 mM HU for 2 h with or without CDC7i. Cells were stained for γH2AX and DNA content. QIBC-derived γH2AX profiles are shown (sample size: 5,361, 4,888, 4,902, and 4,619 cells), and γH2AX levels from cells in S-phase are additionally shown as box plots with white lines indicating the median. **(K)** Western blot analysis of DNA damage markers in cells treated as in J. Mann–Whitney U test in J. A.U., arbitrary units.

consistent with elevated RS upon checkpoint impairment. In agreement, short-term inhibition of CHK1 (using the low-dose CHK1i that on its own does not cause immediate DNA damage) greatly sensitized cells to HU, but only moderately affected the response to camptothecin (CPT; Fig. 4, A–C; and Fig. S3, C and D). To uncouple CHK1 inhibition from CHK1i-induced CHK1 destabilization, we treated cells for 2 h with CHK1i, and then washed out the drug before exposing cells to HU (Fig. 4, D–F). This resulted in reduced CHK1 levels (Fig. 4 F), yet largely restored HU-induced activation of the remaining CHK1 (Fig. 4 E). Also in these conditions, the cells that had been exposed to CHK1i were hypersensitive to HU-induced RS (Fig. 4, D and F). Moreover, to further dissociate the effect of CHK1i-induced CHK1 degradation from CHK1i-induced origin firing, we combined the CHK1i pulse with CDC7 inhibition to block activation of new origins and thereby abrogate this branch of CHK1i functions (Fig. S3, E–G). CHK1i-exposed cells were hypersensitive to acute RS also in these conditions, despite the fact that the remaining CHK1 pool was efficiently activated by HU (Fig. 4, G–I; and Fig. S3, H–K). The sensitization was milder compared with the conditions without CDC7i, consistent with the notion that hyperactivation of origin firing by CHK1i is a major contributor to RS sensitivity. Collectively, these experiments suggest that lowered CHK1 levels, upon impaired steady-state CHK1 activity and the ensuing CHK1 degradation, are insufficient to properly maintain S-phase checkpoint functions. Keeping cells exposed to CDC7i during the complete duration of the experiment largely rescued this effect (Fig. 4, J and K), indicating that unscheduled activation of replication origins upon lowered CHK1 levels drive RS sensitivity. These findings are in agreement with previous studies demonstrating CHK1 haploinsufficiency (Lam et al., 2004; Boles et al., 2010) and suggest that reductions in CHK1 levels, even during unperturbed DNA replication, affect the replication program and can sensitize cells to RS. In summary, we therefore propose that a failure to maintain an autoactivatory loop of basal CHK1 activity and stability turns this loop into a vicious cycle of CHK1 destabilization, impaired intrinsic S-phase checkpoint functions, accumulation of RS and DNA damage, and eventually elimination of affected cells from the proliferative pool (Fig. 5).

Using controlled conditions of CHK1 inhibition allowed us to unveil an autoactivatory mechanism by which cells ensure maintenance functions of this essential kinase during unperturbed cell cycle progression. Our results show that reduced CHK1 activity does not result in immediate DNA damage. Rather, the inability to promote its own phosphorylation leads to CHK1 destabilization and gradual decrease of CHK1 levels. We thus propose that an autoactivatory mechanism prevents a negative circuit of CHK1 degradation, loss of intrinsic checkpoint functions, compromised capability to respond to RS, and decreased replication capacity.

Loss of checkpoint activity has previously been shown to promote CHK1 protein destabilization (Collis et al., 2007; Lin et al., 2014). However, under conditions of complete loss of checkpoint function, CHK1 destabilization co-occurs with and therefore cannot be easily uncoupled from the associated DNA damage. Indeed, exogenous genotoxic assaults can target CHK1 for proteasomal degradation as a means to actively terminate checkpoint signaling and allow cells to resume cell cycle progression (Zhang et al., 2005). Different from such a scenario of checkpoint termination, our results illustrate that during normal cell proliferation and in the absence of DNA damage, a threshold of basal CHK1 activity is actually required to maintain its stability. In line with this notion, we envision a broad spectrum of conditions in which CHK1 activation, e.g., by defects in the upstream signaling, is impaired and in which reduced CHK1 stability will render cells hypersensitive to RS treatments.

The molecular signals needed to maintain the CHK1 autoactivatory loop during unperturbed cell proliferation remain poorly defined and are a subject for further research. Somewhat surprisingly, our cell cycle–resolved single cell analyses of CHK1 basal activity and stability suggest that this regulatory circuit is not confined to the S-phase, but instead operates throughout the cell cycle. We thus reason that DNA replication might not be the sole cellular signal that maintains CHK1 activity and stability. RPA, which functions as a key sensor of ssDNA and creates a platform for ATR/CHK1 activation, was previously shown to bind to transcriptionally active gene regulatory elements independently of the cell cycle position, suggesting that ssDNA is present at sites of transcription (Sikorski et al., 2011; Nguyen et al., 2017; Zhang et al., 2017). It is thus tempting to speculate that transcriptional activity could play a role in promoting basal ATR/CHK1 activity. Further work will be needed to mechanistically dissect how alterations in transcription or mRNA biogenesis affect intrinsic S-phase checkpoint functions in contexts beyond DNA replication. Interestingly, the ability of ETAA1 to bind directly to RPA distinguishes it from TOPBP1, which requires a free 5′ end at ssDNA–dsDNA junctions, e.g., upon DNA breakage-induced DNA end resection, for recruitment via the MRE11-RAD50-NBS1 and 9-1-1 complexes (Saldivar et al., 2017). Therefore, ETAA1 and TOPBP1 likely have both overlapping as well as distinct functions in S-phase checkpoint control, with ETAA1 promoting steady-state ATR/CHK1 activity and controlling origin activation in unchallenged conditions and TOPBP1 playing a more dominant role upon acute and more severe RS and when cells experience DNA damage during S-phase progression.

Impaired CHK1 function, regardless of the upstream defect, comes with the risk of deregulated cell cycle control, replication problems, and RS-associated DNA damage. We suggest that CHK1 destabilization by proteasomal degradation when its basal activity cannot be maintained might be a common outcome of multiple settings of checkpoint malfunction and
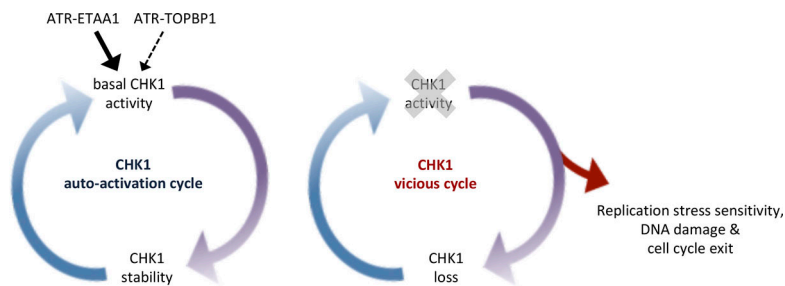
Figure 5. **Working model of CHK1 regulation.** CHK1 activity safeguards CHK1 stability during normal cell proliferation. This autoactivation cycle can turn into a vicious cycle of CHK1 de-stabilization upon impaired CHK1 activity, which leads to compromised checkpoint functions, RS sensitivity, and eventually DNA damage and cell cycle exit.

that it provides a general safeguard mechanism to eliminate severely compromised cells with persistently impaired checkpoint function from the proliferative cell pool. Given the frequent down-regulation of p53 and p21 in cancer, this safeguard mechanism might become deactivated during carcinogenesis, thus allowing checkpoint-impaired cells to continue proliferate and accumulate mutations. Knowing the cellular thresholds at which ATR and CHK1 inhibitors lead to CHK1 destabilization without causing massive DNA damage in S-phase might be of help to better define the therapeutic windows for these essential protein kinase inhibitors.

Materials and methods

Cell culture, drug treatments, and 5-ethynyl-2'-desoxyuridine (EdU) labeling

Cells were grown in a sterile cell culture environment and routinely tested for mycoplasma contamination. Human U-2 OS cells, hTERT-RPE1 cells, and HeLa cells (all of female origin) were grown under standard cell culture conditions (humidified atmosphere, 5% CO_2) in DMEM containing 10% FBS (GIBCO) and penicillin-streptomycin antibiotics. U-2 OS TetOn cells (kindly provided by A. Zubiaga) stably expressing CHK1 were generated by transfection of pTRE2hyg2-HA containing the CHK1 sequence (WT, S296A, or D130A). Induction of CHK1 expression was achieved by doxycycline treatment (1,000 ng/ml). All cultured cells were routinely assessed by QIBC for proper proliferation and absence of abnormal stress signals using cell cycle–resolved profiles of CyclinA, CyclinB, 53BP1, and RPA foci, as well as nuclear morphology and EdU incorporation as readouts. Plasmid transfections were performed with Lipofectamine 3000 (Thermo Fisher Scientific) according to the manufacturer's recommendations. For pulsed EdU (Thermo Fisher Scientific) incorporation, cells were incubated for 20 min in medium containing 10 µM EdU. The Click-iT EdU Alexa Fluor Imaging Kit (Thermo Fisher Scientific) was used for EdU detection. Unless stated otherwise, the following compounds were used at the indicated final concentrations: UCN-01 (30–300 nM; U6508; Sigma-Aldrich), MG132 (10 µM; M7449; Sigma-Aldrich), cycloheximide (50 µM; C7698; Sigma-Aldrich), CHIR-124 (5–50 nM; S2683; Selleckchem), CPT (50 nM to 1 µM; S1288; Selleckchem), HU (0.1–2 mM; H8627; Sigma-Aldrich), CDC7i PHA-767491 (20 µM; S2742; Selleckchem), and roscovitine (20 µM; S1153; Selleckchem). Irradiation was performed with a Faxitron Cabinet x-ray System Model RX-650.

siRNA transfections

siRNA transfections were performed for 24–72 h as indicated with Ambion Silencer Select siRNAs using Lipofectamine RNAiMAX (Thermo Fisher Scientific). The following Ambion Silencer Select siRNAs were used: CHK1 (s502): 5′-GACACGAUU CUUUACCAAA-3′; DDB1 (s3981): 5′-GAGAUUGCUCGAGACUUU A-3′; ETAA1 #A (s29020): 5′-GUAAAACCAGUGUUAGUAA-3′; ETAA1 #B (s29019): 5′-GACUAGUGCAUCAAAAGUA-3′; ETAA1 #C (s29018): 5′-GCAUGUCAUCAAUUAGAUA-3′; ATR (s536): 5′-UUGUAGAAAUGGAUACUGA-3′; TOPBP1 (s21824): 5′-GCAGAA CUGUUGCGGAUUA-3′.

Unless stated otherwise, ETAA1 #A (s29020) was used for ETAA1 depletions. Negative Silencer Select control Neg1 from Ambion was used as nontargeting control and is abbreviated siCon in the figures. For individual siRNA transfections, a final siRNA concentration of 25 nM was used unless stated otherwise. CHK1 depletion was performed at a final siRNA concentration of 0.2 nM. When several siRNAs were combined, the final siRNA concentration was identical for all conditions within one experiment. The siRNA-based screen was performed by reverse-transfection of U-2 OS cells cultured in CELLSTAR 96-well plates (Greiner Bio-One) with Ambion Silencer Select siRNAs at a final concentration of 5 nM using HiPerFect (Qiagen) reagent.

RNA extraction and quantitative PCR (qPCR)

RNA was purified with TRIzol reagent (Life Technologies). RNA was primed with random hexamers (11034731001; Roche) and reverse-transcribed to cDNA using a MultiScribe Reverse transcription (4311235; Thermo Fisher Scientific). qPCR was performed with KAPA SYBR FAST qPCR Kit (KAPA Biosystems) on a Rotor Gene Q system (Qiagen). Samples were run in triplicates and normalized to EIF2C2, and results are depicted as relative fold changes. The following primer pairs were used: CHK1 forward: 5′-AAAGGGATAACCTCAAAATCTCAGACT-3′; CHK1 reverse: 5′-ATACCGAAATACTGTTGCCAAGC-3′; EIF2C2 forward: 5′-GTCCCTTTTGAGACGATCCAG-3′; EIF2C2 reverse: 5′-AGC CAAACCACACTTCTCG-3′.

Immunochemical methods

Proteins were resolved by SDS-PAGE and transferred onto polyvinylidene fluoride membranes. Membranes were blocked with PBS-Tween 20 (0.01%) containing 5% milk powder for 1 h at room temperature. Primary antibodies in blocking solution were applied overnight at 4°C. The following primary antibodies were used for Western blot analysis: CHK1 (1:1,000; rabbit; ab40866; Abcam), CHK1 phospho S296 (1:500; rabbit; ab79758;

Abcam), CHK1 phospho S317 (1:500; rabbit; 2344; Cell Signaling), CHK1 phospho S345 (1:500; rabbit; 2348; Cell Signaling), ETAA1 (1:500; rabbit; ab122245; Abcam), DDB1 (1:2,000; rabbit; ab109027; Abcam), TOPBP1 (1:1,000; rabbit; ab2402; Abcam), RPA32 phospho S4/8 (1:500; rabbit; A300-245A; Bethyl), KAP1 phospho S824 (1:500; rabbit; ab70369; Abcam), KAP1 (1:1,000; rabbit; A300-274A; Bethyl), PCNA (1:1,000; mouse; sc-56; Santa Cruz), tubulin (1:2,000; mouse; T6199; Sigma-Aldrich), and HA (1:500; mouse; 901513; Biolegend). Secondary horseradish peroxidase–coupled antibodies (Vector Laboratories and Thermo Fisher Scientific) were applied for 1 h at room temperature in PBS-Tween 20 (0.01%) containing 1% milk powder before detection by ECL-based chemiluminescence.

Immunostaining

Cells were grown on sterile 12-mm glass coverslips, fixed in 3% formaldehyde in PBS for 15 min at room temperature, washed once in PBS, permeabilized for 5 min at room temperature in PBS supplemented with 0.2% Triton X-100 (Sigma-Aldrich), and washed twice in PBS. All primary antibodies (see below for specifications) and secondary antibodies (Alexa fluorophores; Life Technologies) were diluted in filtered DMEM containing 10% FBS and 0.02% sodium azide. Antibody incubations were performed for 1–2 h at room temperature. After antibody incubations, coverslips were washed once with PBS and incubated for 10 min with PBS containing DAPI (0.5 µg/ml) at room temperature to stain DNA. Following three washing steps in PBS, coverslips were briefly washed with distilled water and mounted on 6 µl Mowiol-based mounting media. The following primary antibodies were used for immunostaining: CHK1 (1:500; rabbit; ab40866; Abcam), CHK1 phospho S296 (1:500; rabbit; ab79758; Abcam), H2AX phospho S139 (1:1,000; mouse; 613401; Biolegend), KAP1 phospho S824 (1:500; rabbit; ab70369; Abcam), RPA32 phospho S4/8 (1:500; rabbit; A300-245A; Bethyl), p21 (1:100; rabbit; sc-756; Santa Cruz), HA (1:500; mouse; 901513; Biolegend), and pH3S10 (rabbit; ab5176; Abcam).

QIBC

Automated multichannel wide-field microscopy for QIBC was performed on an Olympus ScanR Screening System equipped with an inverted motorized Olympus IX83 microscope, a motorized stage, infrared-laser hardware autofocus, a fast emission filter wheel with single band emission filters, and a digital monochrome Hamamatsu ORCA-FLASH 4.0 V2 sCMOS camera (2,048 × 2,048 pixels, 12-bit dynamics). For each condition, image information of large cohorts of cells (typically at least 500 cells for the UPLSAPO 40× objective [NA 0.9], at least 2,000 cells for the UPLSAPO 20× objective [NA 0.75], and at least 5,000 cells for the UPLSAPO 10× [NA 0.4] and UPLSAPO 4× [NA 0.16] objectives) was acquired under nonsaturating conditions at a single autofocus-directed z-position. Identical settings were applied to all samples within one experiment. Images were analyzed with the inbuilt Olympus ScanR Image Analysis Software Version 3.0.0, a dynamic background correction was applied, and nuclei segmentation was performed using an integrated intensity-based object detection module based on the DAPI signal. All downstream analyses were focused on properly detected interphase nuclei containing a 2C-4C

DNA content as measured by total and mean DAPI intensities. Unless stated otherwise, mitotic cells with condensed chromosomes based on high mean DAPI were excluded from the quantifications. Fluorescence intensities were quantified and are depicted as arbitrary units. Color-coded scatter plots of asynchronous cell populations were generated with Spotfire data visualization software (TIBCO) and GraphPad Prism 8.0 for depicting the data as violin plots. Within one experiment, similar cell numbers were compared for the different conditions. Representative scatter plots and quantifications of independent experiments, typically containing several thousand cells each, are shown.

Coimmunoprecipitation

To assess ubiquitin levels of CHK1, cells transfected with a plasmid expressing Flag-ubiquitin were collected in RIPA buffer (50 mM Tris, pH 8, 150 mM NaCl, 1% Igepal CA-630, 0.1% SDS, and 0.1% Na-deoxycholic acid) supplemented with 2 mM MgCl$_2$, 25 U/ml benzonase (71206–3; Merck), 1× protease inhibitor cocktail (cOmplete; Roche), 1× phosphatase inhibitor cocktail (PhosSTOP; Roche), and 10 mM N-ethylmaleimide. 10% of the volume was kept for input controls. 600 µg of protein was subjected to immunoprecipitation for 3 h at 4°C using CHK1 antibody (1 µg per sample; rabbit; ab40866; Abcam) coupled to 15 µl of equilibrated beads (Protein G Sepharose 4 Fast Flow; 17-0618-01; GE). Precipitates were washed three times with immunoprecipitation buffer, separated on a 10% SDS–polyacrylamide gel, and analyzed by immunoblot.

DNA fiber analysis

Cells were pulse-labeled during the last hour of the indicated treatments with 38 µM CldU (Sigma-Aldrich) and 340 µM IdU (European Pharmacopoeia) for 30 min each. Cells were collected and resuspended in PBS at 3 × 10^5 cells per ml. The labeled cells were diluted 2:1 (vol/vol) with unlabeled cells, and 3 µl of cell suspension were mixed with 7 µl of lysis buffer (200 mM Tris-HCl, pH 7.5, 50 mM EDTA, and 0.5% [wt/vol] SDS) on a glass slide. After 9 min, the slide was tilted to 15–45°, and the resulting DNA spreads were air-dried and fixed in methanol/acetic acid (3:1) solution overnight at 4°C. The fibers were denatured with 2.5 M HCl for 60 min, washed several times with PBS to neutralize the pH, and blocked with 0.1% Tween 20 in 2% BSA/PBS for 40 min. The newly replicated CldU and IdU tracks were labeled for 2.5 h at room temperature with anti-BrdU antibodies recognizing CldU (1:400; rat; ab6326; Abcam) and IdU (1:80; mouse; 347580 B44; BD), followed by a 1.5-h incubation with secondary antibodies at room temperature in the dark: anti-mouse Alexa Fluor 488 (1:250; A11001; Invitrogen) and anti-rat Cy3 (1:250, 712-166-153; Jackson ImmunoResearch Laboratories). Fibers were visualized on a Leica DMI 6000 inverted microscope using an HCX Plan APO DIC 63× oil objective (1.4–0.6 NA) and analyzed using Fiji. At least 100 fibers were analyzed per replicate condition. Origins of replication initiating during the first pulse with CldU (detected in red) and extending in both directions from the point of initiation as determined by the subsequent bidirectional incorporation of IdU (detected in green) were scored from at least 100 fibers per condition in

technical duplicates from two independent experiments, and the results are depicted as means ± SD.

Statistical analysis

QIBC-derived quantifications are depicted as violin plots with median (solid line) and quartiles (dashed lines) indicated, or as box plots of the interquartile range with medians indicated (white lines), whiskers denoting the 1.5 × interquartile range range, and outliers shown as individual data points. DNA fiber length measurements are shown as scatter plots with means ± SD. Replication initiation events are depicted as means ± SD, and individual data points are shown in the same graph. qPCR data are presented as means ± SD. The Mann–Whitney U test was used to compare QIBC data and replication fork speed measurements. The unpaired t test was used for qPCR, Western blot, and origin firing data. GraphPad Prism Version 8.0 was used for all statistical analyses; $P < 0.05$ was considered significant and $P \geq 0.05$ was considered not significant.

Online supplemental material

Fig. S1 contains additional data panels on CHK1 steady-state activity regulating CHK1 stability and is mainly related to Fig. 1. Fig. S2 contains additional data panels on upstream regulators of CHK1 activity and stability and is mainly related to Figs. 2 and 3. Fig. S3 contains additional data panels on consequences of CHK1 degradation upon impaired steady-state activity and is mainly related to Fig. 4. Table S1 provides individual z-scores for CHK1 levels upon siRNA-mediated knockdowns related to the screen results depicted in Fig. 3 A.

References

Alonso-de Vega, I., Y. Martín, and V.A. Smits. 2014. USP7 controls Chk1 protein stability by direct deubiquitination. *Cell Cycle.* 13:3921–3926. https://doi.org/10.4161/15384101.2014.973324

Altmeyer, M., L. Toledo, T. Gudjonsson, M. Grøfte, M.B. Rask, C. Lukas, V. Akimov, B. Blagoev, J. Bartek, and J. Lukas. 2013. The chromatin scaffold protein SAFB1 renders chromatin permissive for DNA damage signaling. *Mol. Cell.* 52:206–220. https://doi.org/10.1016/j.molcel.2013.08.025

Bass, T.E., J.W. Luzwick, G. Kavanaugh, C. Carroll, H. Dungrawala, G.G. Glick, M.D. Feldkamp, R. Putney, W.J. Chazin, and D. Cortez. 2016. ETAA1 acts at stalled replication forks to maintain genome integrity. *Nat. Cell Biol.* 18:1185–1195. https://doi.org/10.1038/ncb3415

Blackford, A.N., and S.P. Jackson. 2017. ATM, ATR, and DNA-PK: The Trinity at the Heart of the DNA Damage Response. *Mol. Cell.* 66:801–817. https://doi.org/10.1016/j.molcel.2017.05.015

Boles, N.C., S. Peddibhotla, A.J. Chen, M.A. Goodell, and J.M. Rosen. 2010. Chk1 haploinsufficiency results in anemia and defective erythropoiesis. *PLoS One.* 5:e8581. https://doi.org/10.1371/journal.pone.0008581

Chen, P., C. Luo, Y. Deng, K. Ryan, J. Register, S. Margosiak, A. Tempczyk-Russell, B. Nguyen, P. Myers, K. Lundgren, et al. 2000. The 1.7 A crystal structure of human cell cycle checkpoint kinase Chk1: implications for Chk1 regulation. *Cell.* 100:681–692. https://doi.org/10.1016/S0092-8674(00)80704-7

Cheng, Y.C., and S.Y. Shieh. 2018. Deubiquitinating enzyme USP3 controls CHK1 chromatin association and activation. *Proc. Natl. Acad. Sci. USA.* 115:5546–5551. https://doi.org/10.1073/pnas.1719856115

Collis, S.J., L.J. Barber, A.J. Clark, J.S. Martin, J.D. Ward, and S.J. Boulton. 2007. HCLK2 is essential for the mammalian S-phase checkpoint and impacts on Chk1 stability. *Nat. Cell Biol.* 9:391–401. https://doi.org/10.1038/ncb1555

den Elzen, N.R., and M.J. O'Connell. 2004. Recovery from DNA damage checkpoint arrest by PP1-mediated inhibition of Chk1. *EMBO J.* 23:908–918. https://doi.org/10.1038/sj.emboj.7600105

Deshar, R., W. Yoo, E.B. Cho, S. Kim, and J.B. Yoon. 2019. RNF8 mediates NONO degradation following UV-induced DNA damage to properly terminate ATR-CHK1 checkpoint signaling. *Nucleic Acids Res.* 47:762–778. https://doi.org/10.1093/nar/gky1166

Dobbelstein, M., and C.S. Sørensen. 2015. Exploiting replicative stress to treat cancer. *Nat. Rev. Drug Discov.* 14:405–423. https://doi.org/10.1038/nrd4553

Eykelenboom, J.K., E.C. Harte, L. Canavan, A. Pastor-Peidro, I. Calvo-Asensio, M. Llorens-Agost, and N.F. Lowndes. 2013. ATR activates the S-M checkpoint during unperturbed growth to ensure sufficient replication prior to mitotic onset. *Cell Reports.* 5:1095–1107. https://doi.org/10.1016/j.celrep.2013.10.027

Gaillard, H., T. García-Muse, and A. Aguilera. 2015. Replication stress and cancer. *Nat. Rev. Cancer.* 15:276–289. https://doi.org/10.1038/nrc3916

Ge, X.Q., and J.J. Blow. 2010. Chk1 inhibits replication factory activation but allows dormant origin firing in existing factories. *J. Cell Biol.* 191:1285–1297. https://doi.org/10.1083/jcb.201007074

González Besteiro, M.A., and V. Gottifredi. 2015. The fork and the kinase: a DNA replication tale from a CHK1 perspective. *Mutat. Res. Rev. Mutat. Res.* 763:168–180. https://doi.org/10.1016/j.mrrev.2014.10.003

Haahr, P., S. Hoffmann, M.A. Tollenaere, T. Ho, L.I. Toledo, M. Mann, S. Bekker-Jensen, M. Räschle, and N. Mailand. 2016. Activation of the ATR kinase by the RPA-binding protein ETAA1. *Nat. Cell Biol.* 18:1196–1207. https://doi.org/10.1038/ncb3422

Huh, J., and H. Piwnica-Worms. 2013. CRL4(CDT2) targets CHK1 for PCNA-independent destruction. *Mol. Cell. Biol.* 33:213–226. https://doi.org/10.1128/MCB.00847-12

Ito, F., C. Yoshimoto, Y. Yamada, T. Sudo, and H. Kobayashi. 2018. The HNF-1β-USP28-Claspin pathway upregulates DNA damage-induced Chk1 activation in ovarian clear cell carcinoma. *Oncotarget.* 9:17512–17522. https://doi.org/10.18632/oncotarget.24776

Jackson, S.P., and T. Helleday. 2016. DNA REPAIR. Drugging DNA repair. *Science.* 352:1178–1179. https://doi.org/10.1126/science.aab0958

Kasahara, K., H. Goto, M. Enomoto, Y. Tomono, T. Kiyono, and M. Inagaki. 2010. 14-3-3gamma mediates Cdc25A proteolysis to block premature mitotic entry after DNA damage. *EMBO J.* 29:2802–2812. https://doi.org/10.1038/emboj.2010.157

Lam, M.H., Q. Liu, S.J. Elledge, and J.M. Rosen. 2004. Chk1 is haploinsufficient for multiple functions critical to tumor suppression. *Cancer Cell.* 6:45–59. https://doi.org/10.1016/j.ccr.2004.06.015

Lee, Y.C., Q. Zhou, J. Chen, and J. Yuan. 2016. RPA-Binding Protein ETAA1 Is an ATR Activator Involved in DNA Replication Stress Response. *Curr. Biol.* 26:3257–3268. https://doi.org/10.1016/j.cub.2016.10.030

Leung-Pineda, V., J. Huh, and H. Piwnica-Worms. 2009. DDB1 targets Chk1 to the Cul4 E3 ligase complex in normal cycling cells and in cells experiencing replication stress. *Cancer Res.* 69:2630–2637. https://doi.org/10.1158/0008-5472.CAN-08-3382

Lin, Y.F., H.Y. Shih, Z. Shang, S. Matsunaga, and B.P. Chen. 2014. DNA-PKcs is required to maintain stability of Chk1 and Claspin for optimal replication stress response. *Nucleic Acids Res.* 42:4463–4473. https://doi.org/10.1093/nar/gku116

Liu, Q., S. Guntuku, X.S. Cui, S. Matsuoka, D. Cortez, K. Tamai, G. Luo, S. Carattini-Rivera, F. DeMayo, A. Bradley, et al. 2000. Chk1 is an essential kinase that is regulated by Atr and required for the G(2)/M DNA damage checkpoint. *Genes Dev.* 14:1448–1459.

Liu, Z., K. Yanagisawa, S. Griesing, M. Iwai, K. Kano, N. Hotta, T. Kajino, M. Suzuki, and T. Takahashi. 2017. TTF-1/NKX2-1 binds to DDB1 and confers replication stress resistance to lung adenocarcinomas. *Oncogene.* 36:3740–3748. https://doi.org/10.1038/onc.2016.524

Ma, Y., D. Cui, X. Xiong, H. Inuzuka, W. Wei, Y. Sun, B.J. North, and Y. Zhao. 2018. SCFbeta-TrCP ubiquitinates CHK1 in an AMPK-dependent manner in response to glucose deprivation. *Mol. Oncol.* 13:307–321.

Mailand, N., S. Bekker-Jensen, J. Bartek, and J. Lukas. 2006. Destruction of Claspin by SCFbetaTrCP restrains Chk1 activation and facilitates recovery from genotoxic stress. *Mol. Cell.* 23:307–318. https://doi.org/10.1016/j.molcel.2006.06.016

Mamely, I., M.A. van Vugt, V.A. Smits, J.I. Semple, B. Lemmens, A. Perrakis, R.H. Medema, and R. Freire. 2006. Polo-like kinase-1 controls proteasome-dependent degradation of Claspin during checkpoint recovery. *Curr. Biol.* 16:1950–1955. https://doi.org/10.1016/j.cub.2006.08.026

Maya-Mendoza, A., E. Petermann, D.A. Gillespie, K.W. Caldecott, and D.A. Jackson. 2007. Chk1 regulates the density of active replication origins during the vertebrate S phase. *EMBO J.* 26:2719–2731. https://doi.org/10.1038/sj.emboj.7601714

Nguyen, H.D., T. Yadav, S. Giri, B. Saez, T.A. Graubert, and L. Zou. 2017. Functions of Replication Protein A as a Sensor of R Loops and a Regulator of RNaseH1. *Mol. Cell.* 65:832–847.

Okita, N., S. Minato, E. Ohmi, S. Tanuma, and Y. Higami. 2012. DNA damage-induced CHK1 autophosphorylation at Ser296 is regulated by an intramolecular mechanism. *FEBS Lett.* 586:3974–3979. https://doi.org/10.1016/j.febslet.2012.09.048

Park, C., Y. Suh, and A.M. Cuervo. 2015. Regulated degradation of Chk1 by chaperone-mediated autophagy in response to DNA damage. *Nat. Commun.* 6:6823. https://doi.org/10.1038/ncomms7823

Peschiaroli, A., N.V. Dorrello, D. Guardavaccaro, M. Venere, T. Halazonetis, N.E. Sherman, and M. Pagano. 2006. SCFbetaTrCP-mediated degradation of Claspin regulates recovery from the DNA replication checkpoint response. *Mol. Cell.* 23:319–329. https://doi.org/10.1016/j.molcel.2006.06.013

Saldivar, J.C., D. Cortez, and K.A. Cimprich. 2017. The essential kinase ATR: ensuring faithful duplication of a challenging genome. *Nat. Rev. Mol. Cell Biol.* 18:622–636. https://doi.org/10.1038/nrm.2017.67

Saldivar, J.C., S. Hamperl, M.J. Bocek, M. Chung, T.E. Bass, F. Cisneros-Soberanis, K. Samejima, L. Xie, J.R. Paulson, W.C. Earnshaw, et al. 2018. An intrinsic S/G_2 checkpoint enforced by ATR. *Science.* 361:806–810. https://doi.org/10.1126/science.aap9346

Schmitt, E., R. Boutros, C. Froment, B. Monsarrat, B. Ducommun, and C. Dozier. 2006. CHK1 phosphorylates CDC25B during the cell cycle in the absence of DNA damage. *J. Cell Sci.* 119:4269–4275. https://doi.org/10.1242/jcs.03200

Shen, J.P., R. Srivas, A. Gross, J. Li, E.J. Jaehnig, S.M. Sun, A. Bojorquez-Gomez, K. Licon, V. Sivaganesh, J.L. Xu, et al. 2015. Chemogenetic profiling identifies RAD17 as synthetically lethal with checkpoint kinase inhibition. *Oncotarget.* 6:35755–35769. https://doi.org/10.18632/oncotarget.5928

Sikorski, T.W., S.B. Ficarro, J. Holik, T. Kim, O.J. Rando, J.A. Marto, and S. Buratowski. 2011. Sub1 and RPA associate with RNA polymerase II at different stages of transcription. *Mol. Cell.* 44:397–409. https://doi.org/10.1016/j.molcel.2011.09.013

Smits, V.A., and D.A. Gillespie. 2015. DNA damage control: regulation and functions of checkpoint kinase 1. *FEBS J.* 282:3681–3692. https://doi.org/10.1111/febs.13387

Sørensen, C.S., and R.G. Syljuåsen. 2012. Safeguarding genome integrity: the checkpoint kinases ATR, CHK1 and WEE1 restrain CDK activity during normal DNA replication. *Nucleic Acids Res.* 40:477–486. https://doi.org/10.1093/nar/gkr697

Syljuåsen, R.G., C.S. Sørensen, L.T. Hansen, K. Fugger, C. Lundin, F. Johansson, T. Helleday, M. Sehested, J. Lukas, and J. Bartek. 2005. Inhibition of human Chk1 causes increased initiation of DNA replication, phosphorylation of ATR targets, and DNA breakage. *Mol. Cell. Biol.* 25:3553–3562. https://doi.org/10.1128/MCB.25.9.3553-3562.2005

Takai, H., K. Tominaga, N. Motoyama, Y.A. Minamishima, H. Nagahama, T. Tsukiyama, K. Ikeda, K. Nakayama, M. Nakanishi, and K. Nakayama. 2000. Aberrant cell cycle checkpoint function and early embryonic death in Chk1(-/-) mice. *Genes Dev.* 14:1439–1447.

Técher, H., S. Koundrioukoff, A. Nicolas, and M. Debatisse. 2017. The impact of replication stress on replication dynamics and DNA damage in vertebrate cells. *Nat. Rev. Genet.* 18:535–550. https://doi.org/10.1038/nrg.2017.46

Toledo, L.I., M. Altmeyer, M.B. Rask, C. Lukas, D.H. Larsen, L.K. Povlsen, S. Bekker-Jensen, N. Mailand, J. Bartek, and J. Lukas. 2013. ATR prohibits replication catastrophe by preventing global exhaustion of RPA. *Cell.* 155:1088–1103. https://doi.org/10.1016/j.cell.2013.10.043

Toledo, L., K.J. Neelsen, and J. Lukas. 2017. Replication Catastrophe: When a Checkpoint Fails because of Exhaustion. *Mol. Cell.* 66:735–749. https://doi.org/10.1016/j.molcel.2017.05.001

Tu, Y., H. Liu, X. Zhu, H. Shen, X. Ma, F. Wang, M. Huang, J. Gong, X. Li, Y. Wang, et al. 2017. Ataxin-3 promotes genome integrity by stabilizing Chk1. *Nucleic Acids Res.* 45:4532–4549. https://doi.org/10.1093/nar/gkx095

Yazinski, S.A., and L. Zou. 2016. Functions, Regulation, and Therapeutic Implications of the ATR Checkpoint Pathway. *Annu. Rev. Genet.* 50:155–173. https://doi.org/10.1146/annurev-genet-121415-121658

Zeman, M.K., and K.A. Cimprich. 2014. Causes and consequences of replication stress. *Nat. Cell Biol.* 16:2–9. https://doi.org/10.1038/ncb2897

Zhang, H., H. Gan, Z. Wang, J.H. Lee, H. Zhou, T. Ordog, M.S. Wold, M. Ljungman, and Z. Zhang. 2017. RPA Interacts with HIRA and Regulates H3.3 Deposition at Gene Regulatory Elements in Mammalian Cells. *Mol. Cell.* 65:272–284. https://doi.org/10.1016/j.molcel.2016.11.030

Zhang, Y.W., D.M. Otterness, G.G. Chiang, W. Xie, Y.C. Liu, F. Mercurio, and R.T. Abraham. 2005. Genotoxic stress targets human Chk1 for degradation by the ubiquitin-proteasome pathway. *Mol. Cell.* 19:607–618. https://doi.org/10.1016/j.molcel.2005.07.019

Zhang, Y.W., J. Brognard, C. Coughlin, Z. You, M. Dolled-Filhart, A. Aslanian, G. Manning, R.T. Abraham, and T. Hunter. 2009. The F box protein Fbx6 regulates Chk1 stability and cellular sensitivity to replication stress. *Mol. Cell.* 35:442–453. https://doi.org/10.1016/j.molcel.2009.06.030